SUN XIURONG
DONG SHIMIN
WANG HONGBO
and
LI WEICHENG

Simulation model of the sucker rod string buckling configuration in vertical well tubing

A new model based on the entire rod string buckling configuration in vertical well tubing is proposed. The buckling configuration for the rod string constrained in vertical wellbores is divided into four sections: the bottom and second suspended sections, the middle helical section and the top suspended section. The mathematical model not only includes the bending differential equations above the four sections, the boundary conditions at two ends, but also the continuity conditions at contact points whose positions are variable. The numerical simulation of the entire rod string buckling configuration is realized through transforming the mathematical model into non-linear algebraic equations solved by a genetic algorithm. The simulation results show that the boundary conditions at the two ends have little effect on the helical buckling configuration, but, however, the boundary condition, especially at the bottom, has a considerable effect on the configurations of the suspended sections. Compared to the previous results, the new model provides a more accurate description of rod string buckling and can simulate a more genuine buckling configuration of the rod string in the downhole.

Keywords: *Sucker rod string, genetic algorithm, Runge-Kutta, boundary constraint, buckling configuration.*

1. Introduction

The method for calculating the critical buckling load of rod string in vertical wellbores is the theoretical basis of predicting and preventing the eccentric wear of rod and tubing. The rod string buckling in the vertical well tubing of petroleum engineering field is equivalent to slender rod buckling in a circular cylinder. Previous studies show that the buckling configuration of the rod string in a vertical well is divided into two categories: the plane (two-dimensional) or approximate plane buckling under the lower axial compression [1-3]; and the spatial (three-dimensional) buckling under the higher axial compression [4-15]. The theory about first-order plane buckling has been studied intensively; however, spatial buckling has developed continuously with more and more complicated problems.

Generally, when considering the effect of the boundary conditions on the configuration of the rod string, the entire spatial buckling of the rod string in a vertical well is composed of four sections: the bottom and second suspended sections, the middle helical section and the top suspended section.

As regards the spatial buckling of the rod string, the formula based on the relationship of axial force and the pitch was obtained by Lubinski under the assumption of isometric spiral [4]. Then the helical buckling of the rod string was developed by different methods [6-9], but remained at the level of weightless helical buckling. Later, some experts began to research the rod string buckling with weight. Mitchell built a relatively new model combining the buckling equation of the rod string and the boundary condition at the bottom end based on the following two points simplification [12]: (1) the equation of the helical section is solved by the way of reduced-order; (2) by only considering the bottom two suspended sections and the middle helical section, not the integral rod string, as the research object. So the entire rod string buckling problem remained unsolved although his buckling theory made significant progress. Afterwards Gao [10] established the helical buckling model and obtained the critical load for one period of the helix, but only considered the middle helical section local relative to the whole as the object of the study, so that the relationship between the buckling equation and the boundary condition was also not established. Similar to Gao, the calculation method of the critical helical buckling load of the rod string in an inclined well was presented by ignoring the bottom and top suspended sections by Tan et al. [16]. Recently, the entire rod string model was built by Huang et al. [17] by the approximate analytic method, which is also based on the simplified equation and used only a rod of length limited due to the limitations of the selected method.

Based on the above unsolved problem and the actual requirements on eccentric wear of rod and tubing, a new model of the entire rod string was established, including the axial distributed load, the boundary conditions at two ends,

Messrs. Sun Xiurong, Dong Shimin*, Wang Hongbo and Li Weicheng, School of Mechanical Engineering, Yanshan University, Qinhuangdao 066 004, China. Email: ysudshm@163.com

the continuity condition at contact points whose positions are variable, and the middle complete differential equation at the helical section instead of the simplified equation. The configuration of the entire rod string was obtained with all the factors considered above. Finally, their interrelationships are also discussed.

2. Mechanical and mathematical model of the entire rod string

The mechanical model of a compressed rod string with weight constrained in the tubing is shown in Fig.1(a). When the axial compression load exceeds a certain critical value, the rod string touches the inner surface of the well as shown in Fig.1(c); with the compression load increasing gradually, the three-dimensional or helical configuration starts to appear under the constraint of the wall as shown in Fig.1(b) and Fig.1(d). In order to research the spatial helical buckling for convenience, the following assumptions and simplifications are considered:

1. The centerline of the wellbore is coincident with the centerline of the rod string in the vertical well.
2. The inner wall of the tubing is rigid, and friction and torque are neglected.
3. The constraint of the rod string at the top end is simplified as being a fixed end or pinned end; the bottom end is simplified as being a sliding fixed end or pinned end.
4. The effects of the connectors are not considered.

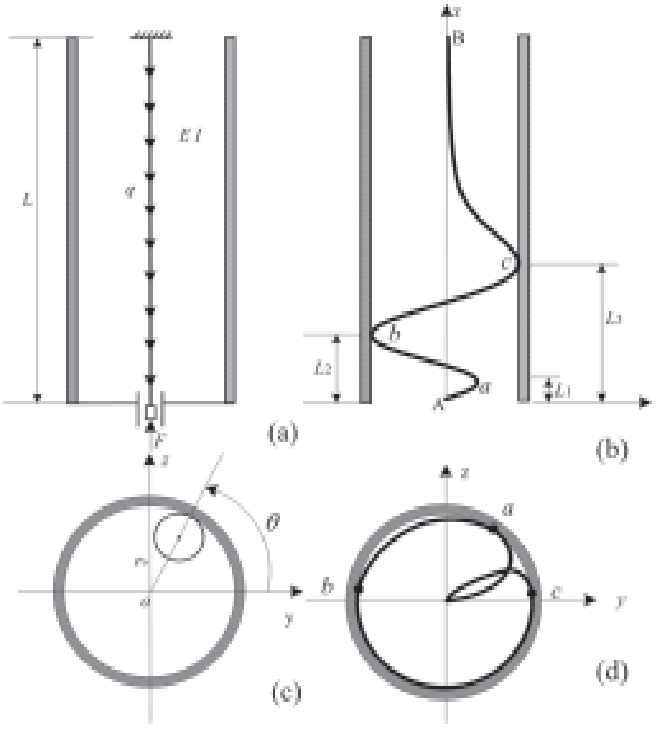

Fig.1 Mechanical model and buckling configuration: (a) The Mechanical model, (b) Buckling configuration, (c) Geometric position of the rod string, (d) The top view of buckling configuration

5. The deformation belongs to linear elastic behaviour with small deformation.
6. The weight of the rod string is an axial distribution load which is regarded as a constant with the unit N/m.

In order to depict the new model, two coordinate systems are established, as shown in Fig.1(b) and Fig.1(d). The rectangular coordinate system is used to describe the bending deformation at the bottom two suspended sections and top suspended section. The polar coordinate system is used to describe the bending deformation of the helical section, namely an arbitrary axial position x corresponds to the angle.

The mathematical model of rod buckling is composed of differential equations corresponding to different sections, boundary conditions at two ends and continuity conditions at the contact points.

2.1 The bending differential equation of the rod string

2.1.1 Buckling equation of the middle helical section

According to the mechanical analysis of the micro-element, the differential equation with the weight rod string in the tubing can be expressed by:

$$\begin{cases} EI\dfrac{d^4y}{dx^4}+\left(F_x\dfrac{dy}{dx}\right)'+N_r\cos\theta=0 \\ EI\dfrac{d^4z}{dx^4}+\left(F_x\dfrac{dz}{dx}\right)'+N_r\sin\theta=0 \end{cases} \quad \ldots \quad (1)$$

where N_r is the contact force per length, *N/m*; F_x is the axial compression of the rod string in section x, $F_x = F\text{-}qx$; F is the pump end load, *N*; E is the elastic modulus, *Pa*; and I is the moment of inertia, m^4.

When Eq(1) is expressed by the polar coordinate system, the helical section buckling equation and contact force equation for the rod string in the tubing are divided into the following two equations independently:

$$EI\theta_x^{(4)}-6EI\theta_x'^2\theta_x''+\left(F_x\theta_x'\right)'=0 \quad \ldots \quad (2)$$

$$N_x=r_0EI\left(-\theta_x'^4+3\theta_x''^2+4\theta_x'\theta_x'''\right)+r_0F_x\theta_x'^2 \quad \ldots \quad (3)$$

Here we let $\omega_0=\sqrt{F/EI}$, by introducing the dimensionless distance $\xi=\omega_0 x$, the dimensionless contact force $n_\xi=N_x/(EIr_0\omega_0^4)$, the dimensionless distribution force per unit length $\varepsilon=\dfrac{q}{EI\omega_0^3}$, Eq(2) and Eq(3) are simplified into their dimensionless forms:

$$\theta_\xi^{(4)}-6\theta_\xi'^2\theta_\xi''+\left[(1-\varepsilon\xi)\theta_\xi'\right]_\xi'=0 \quad \ldots \quad (4)$$

$$n_\xi = 4\theta'_\xi\theta'''_\xi + 3\theta''^2_\xi - \theta'^4_\xi + (1-\varepsilon\xi)\theta'^2_\xi \quad \text{... (5)}$$

In previous studies, Mitchell et al. (1988) and Huang et al (2016) simplified Eq(4) and Eq(5), namely, $\theta_\xi^{\cdot\cdot}$ and the integral constant obtained by the first order integral of Eq(4), and $\theta_\xi^{\cdot\cdot}$, $\theta_\xi^{\cdot\cdot}$ in Eq(5) are all neglected. Then Eq(4) and Eq(5) are replaced by the following forms:

$$\theta'_\xi = \sqrt{(1-\varepsilon\xi)/2} \quad \text{... (6)}$$

$$n_\xi = -\theta'^4_\xi + (1-\varepsilon\xi)\theta'^2_\xi \quad \text{... (7)}$$

2.1.2 Buckling equation of the bottom suspended section

For the bottom suspended section, the contact force N_r is zero. So the differential equation for the bottom suspended section is given by Eq. (1) as follows:

$$\begin{cases} EI\dfrac{d^4y}{dx^4} + \dfrac{d}{dx}\left((F-qx)\dfrac{dy}{dx}\right) = 0 \\ EI\dfrac{d^4z}{dx^4} + \dfrac{d}{dx}\left((F-qx)\dfrac{dz}{dx}\right) = 0 \end{cases} \quad \text{... (8)}$$

By introducing the dimensionless distance $u = \omega_0 y$, $v = \omega_0 z$, $\xi = \omega_0 x$, Eq(8) is simplified into its dimensionless form:

$$\begin{cases} \dfrac{d^4u}{d\xi^4} + \dfrac{d}{d\xi}\left((1-\varepsilon\xi)\dfrac{du}{d\xi}\right) = 0 \\ \dfrac{d^4v}{d\xi^4} + \dfrac{d}{d\xi}\left((1-\varepsilon\xi)\dfrac{dv}{d\xi}\right) = 0 \end{cases} \quad (0 \le \xi \le \xi_1) \quad \text{... (9)}$$

2.1.3 Buckling equation of the second suspended section

It is similar to Eq. (8) and Eq. (9), and the differential equation for the second suspended section is given by Eq. (1) as follows:

$$\begin{cases} \dfrac{d^4u}{d\xi^4} + \dfrac{d}{d\xi}\left((1-\varepsilon\xi)\dfrac{du}{d\xi}\right) = 0 \\ \dfrac{d^4v}{d\xi^4} + \dfrac{d}{d\xi}\left((1-\varepsilon\xi)\dfrac{dv}{d\xi}\right) = 0 \end{cases} \quad (\xi_1 \le \xi \le \xi_2) \quad \text{... (10)}$$

2.1.4 Buckling equation of the top suspended section

Similarly, the differential equation for the top suspended section is given by Eq. (1) as follows:

$$\begin{cases} \dfrac{d^4u}{d\xi^4} + \dfrac{d}{d\xi}\left((1-\varepsilon\xi)\dfrac{du}{d\xi}\right) = 0 \\ \dfrac{d^4v}{d\xi^4} + \dfrac{d}{d\xi}\left((1-\varepsilon\xi)\dfrac{dv}{d\xi}\right) = 0 \end{cases} \quad (\xi_3 \le \xi \le \xi_L) \quad \text{... (11)}$$

2.2 Boundary conditions at the two ends

The boundary conditions at the two fixed ends are given as follows:

$$\begin{cases} u_{A,B} = v_{A,B} = 0 \\ u'_{A,B} = v'_{A,B} = 0 \end{cases} \quad \text{... (12)}$$

The boundary conditions at the two pinned ends are given as follows:

$$\begin{cases} u_{A,B} = v_{A,B} = 0 \\ u''_{A,B} = v''_{A,B} = 0 \end{cases} \quad \text{... (13)}$$

2.3 Continuity conditions at the contact points

The continuity conditions at the contact points *a*, *b* and *c* include geometrical continuity condition (displacement and rotation), moment continuity condition, and tangential equilibrium conditions. The continuity condition at the contact point *a* is expressed by:

$$\begin{cases} y_{a+} = r_0\cos\theta_a \\ z_{a+} = r_0\sin\theta_a \\ y'_{a+} = -r_0\sin\theta_a\theta'_a \\ z'_{a+} = r_0\cos\theta_a\theta'_a \end{cases} \quad \text{... (14)}$$

$$\begin{cases} y_{a-} = r_0\cos\theta_a \\ z_{a-} = r_0\sin\theta_a \\ y'_{a-} = -r_0\sin\theta_a\theta'_a \\ z'_{a-} = r_0\cos\theta_a\theta'_a \end{cases} \quad \text{... (15)}$$

$$\begin{cases} y''_{a-} = y''_{a+} \\ z''_{a-} = z''_{a+} \\ \begin{bmatrix} EIy'''_{a-} + (F-qx_a)y'_{a-} - EIy'''_{a+} \\ -(F-qx_{a+})y'_{a+} \end{bmatrix}\sin\theta_a \\ = \begin{bmatrix} EIz'''_{a-} + (F-qx_a)z'_{a-} - EIz'''_{a+} \\ -(F-qx_{a+})z'_{a+} \end{bmatrix}\cos\theta_a \end{cases} \quad \text{... (16)}$$

Eqs. (14-16) are simplified into dimensionless form as follows:

$$\begin{cases} u_{a+} = r_0\omega_0\cos\theta_a \\ v_{a+} = r_0\omega_0\sin\theta_a \\ u'_{a+} = -r_0\omega_0\sin\theta_a\theta'_a \\ v'_{a+} = r_0\omega_0\cos\theta_a\theta'_a \end{cases} \quad \text{... (17)}$$

$$\begin{cases} u_{a-} = r_0\omega_0\cos\theta_a \\ v_{a-} = r_0\omega_0\sin\theta_a \\ u'_{a-} = -r_0\omega_0\sin\theta_a\theta'_a \\ v'_{a-} = r_0\omega_0\cos\theta_a\theta'_a \end{cases} \quad \text{... (18)}$$

$$\begin{cases} u''_{a+} = u''_{a-} \\ v''_{a+} = v''_{a-} \\ \begin{bmatrix} u'''_{a-} + (1-\varepsilon\xi_a)u'_{a-} - u'''_{a+} \\ -(1-\varepsilon\xi_a)u'_{a+} \end{bmatrix} \sin\theta_a \\ = \begin{bmatrix} v'''_{a-} + (1-\varepsilon\xi_a)v'_{a-} - v'''_{a+} \\ -(1-\varepsilon\xi_a)v'_{a+} \end{bmatrix} \cos\theta_a \end{cases} \quad \ldots (19)$$

The continuity condition at the contact point b is expressed by:

$$\begin{cases} u_b = r_0\omega_0\cos\theta_b \\ v_b = r_0\omega_0\sin\theta_b \\ u'_b = -r_0\omega_0\sin\theta_b\theta'_b \\ v'_b = r_0\omega_0\cos\theta_b\theta'_b \\ u''_b = -r_0\omega_0\cos\theta_b\theta'^2_b - r_0\omega_0\sin\theta_b\theta''_b \\ v''_b = -r_0\omega_0\sin\theta_b\theta'^2_b + r_0\omega_0\cos\theta_b\theta''_b \\ \begin{bmatrix} u'''_b + (1-\varepsilon\xi_b)u'_b - (r_0\omega_0\sin\theta_b\theta'^3_b \\ -3r_0\omega_0\cos\theta_b\theta'_b\theta''_b - r_0\omega_0\sin\theta_b\theta'''_b) \\ +(1-\varepsilon\xi_b)r_0\omega_0\sin\theta_b\theta'_b \end{bmatrix} \sin\theta_b \\ = \begin{bmatrix} v'''_b + (1-\varepsilon\xi_a)v'_b - (-r_0\omega_0\cos\theta_b\theta'^3_b \\ -3r_0\omega_0\sin\theta_b\theta'_b\theta''_b + r_0\omega_0\cos\theta_b\theta'''_b) \\ -(1-\varepsilon\xi_b)r_0\omega_0\cos\theta_b\theta'_b \end{bmatrix} \cos\theta_b \end{cases} \quad \ldots (20)$$

The continuity condition at the contact point c is expressed by:

$$\begin{cases} u_c = r_0\omega_0\cos\theta_c \\ v_c = r_0\omega_0\sin\theta_c \\ u'_c = -r_0\omega_0\sin\theta_c\theta'_c \\ v'_c = r_0\omega_0\cos\theta_c\theta'_c \\ u''_c = -r_0\omega_0\cos\theta_c\theta'^2_c - r_0\omega_0\sin\theta_c\theta''_c \\ v''_c = -r_0\omega_0\sin\theta_c\theta'^2_c + r_0\omega_0\cos\theta_c\theta''_c \\ \begin{bmatrix} u'''_c + (1-\varepsilon\xi_c)u'_c - (r_0\omega_0\sin\theta_c\theta'^3_c \\ -3r_0\omega_0\cos\theta_c\theta'_c\theta''_c - r_0\omega_0\sin\theta_c\theta'''_c) \\ +(1-\varepsilon\xi_c)r_0\omega_0\sin\theta_c\theta'_c \end{bmatrix} \sin\theta_c \\ = \begin{bmatrix} v'''_c + (1-\varepsilon\xi_c)v'_c - (-r_0\omega_0\cos\theta_c\theta'^3_c \\ -3r_0\omega_0\sin\theta_c\theta'_c\theta''_c + r_0\omega_0\cos\theta_c\theta'''_c) \\ -(1-\varepsilon\xi_c)r_0\omega_0\cos\theta_c\theta'_c \end{bmatrix} \cos\theta_c \end{cases} \quad \ldots (21)$$

3. Numerical simulation method

Eqs. (9-11) are the fourth-order homogeneous linear ordinary differential equations with variable coefficients; thus the analytic solution can be derived directly, and also can be calculated by the numerical integral method; Eq(4) is a sophisticated fourth-order non-linear ordinary differential equation, but it seems impossible to obtain an analytical solution under the non-simplified condition, so the numerical solution seems to be the only choice. In this paper, the numerical simulation model is established by Eqs. (4-5) and Eqs. (8-21). The helical section equation and the suspended section equations are solved by the Runge-Kutta method, and the specific simulation algorithm with the boundary conditions at two ends and the contact points are given as follows:

1. The unknown quantity L_1, L_2, L_3 are expressed as x_1, x_2 and x_3, namely, $x_1=L_1$, $x_2=L_2$ and $x_3=L_3$.
2. The boundary conditions at the point *A* and *a* of the bottom suspended section are expressed by:

$$\begin{cases} \{y_A, y'_A, y_a, y'_a\} = \{0, 0, x_4, x_5\} \\ \{z_A, z'_A, z_a, z'_a\} = \{0, 0, x_6, x_7\} \end{cases} \quad \ldots (22)$$

Arbitrarily given a set of values x_1, x_2, x_3, x_4, x_5, x_6, x_7, Eq. (9) can be solved and the simulation results of bottom suspended section at the point *a* can be obtained as follows:

$$\begin{cases} \{y_{a-}, y'_{a-}, y''_{a-}, y'''_{a-}\} \\ \{z_{a-}, z'_{a-}, z''_{a-}, z'''_{a-}\} \end{cases} \quad \ldots (23)$$

3. The boundary condition at the point *a* of the second suspended section is expressed by:

$$\begin{cases} \{y_{a+}, y'_{a+}, y''_{a+}, y'''_{a+}\} = \{r_0\cos x_8, -r_0 x_9\sin x_8, x_{10}, x_{11}\} \\ \{z_{a+}, z'_{a+}, z''_{a+}, z'''_{a+}\} = \{r_0\sin x_8, r_0 x_9\cos x_8, x_{12}, x_{13}\} \end{cases} \quad \ldots (24)$$

where $x_8 = \theta_a$ and $x_9 = \theta'_{a-}$.

Similar to Eq(23), the simulation result of the second suspended section at the point *b* can be obtained by solving Eq(10) as follows:

$$\begin{cases} \{y_{b-}, y'_{b-}, y''_{b-}, y'''_{b-}\} \\ \{z_{b-}, z'_{b-}, z''_{b-}, z'''_{b-}\} \end{cases} \quad \ldots (25)$$

4. The boundary condition at the point *b* of helical section is expressed by

$$\{\theta_b, \theta'_b, \theta''_b, \theta'''_b\} = \{x_{14}, x_{15}, x_{16}, x_{17}\} \quad \ldots (26)$$

Similarly, the simulation results of helical section at the point *c* can be obtained by solving Eq(11) as follows:

$$\{\theta_c, \theta'_c, \theta''_c, \theta'''_c\} \quad \ldots (27)$$

5. The boundary condition at the point '*B*' and '*b*' of top suspended section is expressed by

$$\begin{cases} \left\{ y_B, y_B^{'}, y_c, y_c' \right\} = \left\{ 0, 0, x_{18}, x_{19} \right\} \\ \left\{ z_B, z_B^{'}, z_c, z_c' \right\} = \left\{ 0, 0, x_{20}, x_{21} \right\} \end{cases} \quad \ldots \quad (28)$$

The simulation results of top suspended section at the point *c* can be obtained by solving Eq(4) as follows:

$$\begin{cases} \left\{ y_c, y_c^{'}, y_c^{''}, y_c^{'''} \right\} \\ \left\{ z_c, z_c^{'}, z_c^{''}, z_c^{'''} \right\} \end{cases} \quad (29)$$

Substituting the simulation results of Eq (23), (25), (27), (29), and the assumed boundary value of $\bar{X} = \left\{ x_1, x_2, \cdots, x_{20}, x_{21} \right\}^T$ into Eqs (18-21), the 21 non-linear algebraic equations with boundary value are obtained as follows:

$$\begin{cases} f_1 = f_1(\bar{X}) = 0 \\ f_2 = f_2(\bar{X}) = 0 \\ \quad \vdots \\ f_{20} = f_{20}(\bar{X}) = 0 \\ f_{21} = f_{21}(\bar{X}) = 0 \end{cases} \quad \ldots \quad (30)$$

The numerical solutions of the non-linear algebraic equations Eq(30) are obtained by the following optimization algorithm:

Design variable:

$$\bar{\boldsymbol{X}} = \left\{ x_1, x_2, \ldots, x_{21} \right\}^T \quad \ldots \quad (31)$$

Objective function: For any given set of boundary values, 21 corresponding functions result in Eq (30). By taking the squared error and minimum as the objective function of optimization design, the objective function is expressed by:

$$M \text{in} G\left(\bar{\boldsymbol{X}} \right) = M \text{in}\left(f_1^{\,2} + f_2^{\,2} + \cdots + f_{21}^{\,2} \right) \quad \ldots \quad (32)$$

Constraint condition: only considering the constraint condition in each design variable itself, that is $x_{imin} < x_i < x_{imax}$ (i=1,2,...,21).

Optimization algorithm: the mathematical model established for the optimal design with unknown boundary value is a constrained non-linear optimization problem, and the optimal solution of Eq(30) can be obtained by the genetic algorithm.

4. Results and discussions

The basic parameters: the diameter of the rod string *D* = 25mm; the elastic modulus *E* = 209GPa; the axial distribution force *q* = 25N/m; radial clearance r_0 = 0.0185m; to ensure the

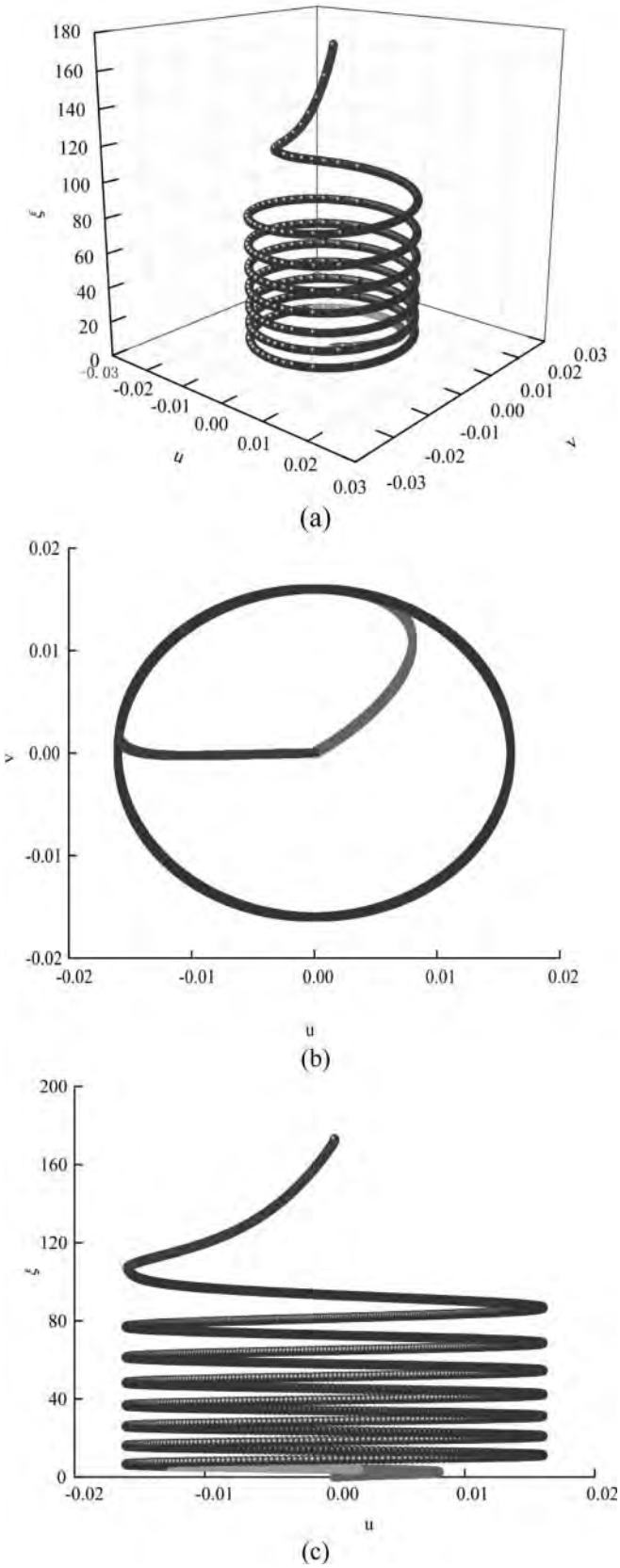

Fig.2 The integral buckling configuration of rod string. (a) the main view, (b) the top view, (c) the front view

neutral point inside the rod string, the rod length is given separately. In the following diagram, F-F represents the fixed boundary at two ends; P-P represents the pinned boundary at two ends.

4.1 Buckling configuration of the rod string

Let L = 200m, F = 3000N, based on the above simulation method, the integral buckling configuration of rod string is obtained with the boundary conditions at two fixed ends as shown in Fig.2.

4.2 Effect of the boundary conditions on the buckling configuration of the rod string

4.2.1 Effect of boundary conditions on the helical section buckling configuration

After obtaining the simulation results of the integral rod string buckling configuration, we extract the helical section buckling configuration for analysis. Fig.3 shows us that the deformation curves under the two fixed ends almost coincides completely with the two pinned ends under the same axial compression load, which indicates that the configuration is effected very little by the boundary conditions.

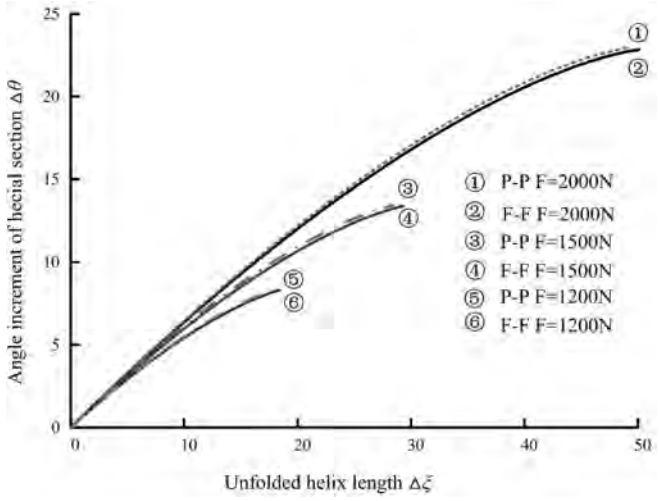

Fig.3 The unfolded curve of helical section

4.2.2 Effect of the boundary conditions on the suspended sections

The derivative of the angle at the cut-in point of the helical section is an important factor which effects the configuration of the helical section and the bottom second suspended section. Fig.4 shows us that the difference of the derivative value of the angle between the two fixed ends and the two pinned ends at contact point *b* is very subtle but great at contact point *a*. The results indicate that the configuration of the helical section is effected very little by the boundary conditions but is affected greatly on the configuration of the bottom suspended section. This is further proved in Fig.5 with the rod length being L = 200m. From Fig.5, we can see that the distance ξ_1 and ξ_2 under the two fixed ends

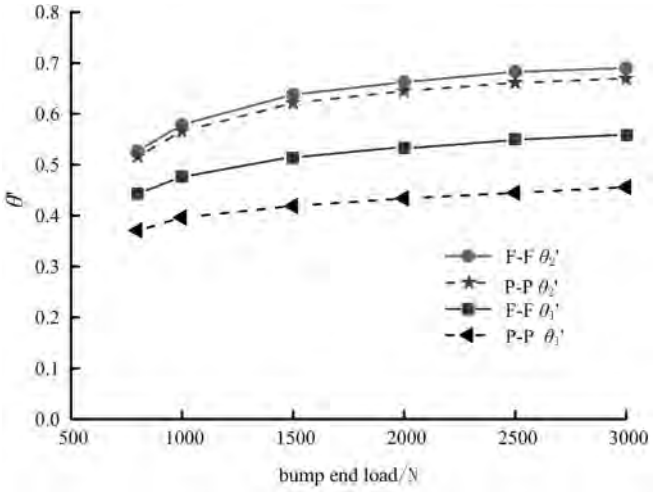

Fig.4 The derivative of angle at contact point changes with the pump end load

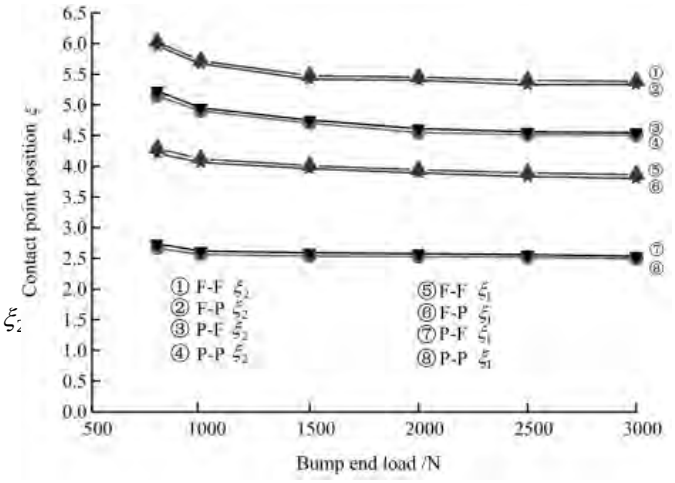

Fig.5 The contact point position changes with the pump end load and boundary constraints

boundaries are both significantly higher than under the two pinned ends boundaries. Further, the distance ξ_1 and is almost coincident with the bottom end boundary though with a different top end boundary. The results indicate that the configurations of suspended sections are effected greatly by the bottom boundary condition but insignificantly by the top boundary condition.

4.3 The law of contact force

The value of the contact force between the rod and tubing determines the degree of the eccentric wear. Fig.6 shows us that the law of change for the contact force at the helical section increases with the increase of the axial compression at the bump end and also different boundary conditions. From Fig.6, we see that the contact force near the beginning of the helical section is somewhat different, but from the whole helical section perspective, the contact force is basically the same under the different boundary conditions P-P and F-F.

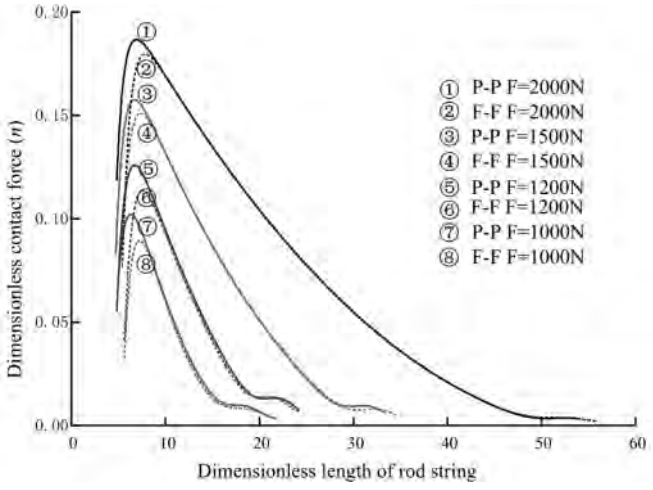

Fig. 6 The contact force comparison results under different boundary conditions

4.4 Comparison with the simplified equation at the helical section

In the previous studies, the equation at the helical section was once simplified to Eqs (6-7). In this paper, the comparison results with the previous ones are given in Fig.7 and Fig.8. We can see that the results of the simplified equation are different from the results of the complete equation which mainly reflected in the beginning and the end of the helical section. Firstly, the contact force near the beginning of the helical section is relatively large in Fig.7; Secondly, the angle increment of the helical section near the end is lower in Fig.8. So the helical buckling simulation results of the simplified equation are larger error compared to the actual buckling condition and is not conducive to compute the rod eccentric wear life. In fact the contact force near the end of the helical section is also different between them, here it is not discussed with little meaning compared to the above factors.

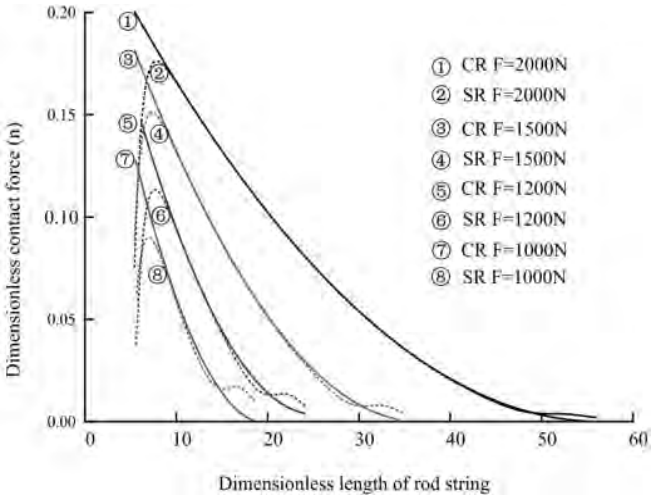

Fig.7 The contact force comparison results between simplified and non-simplified equation

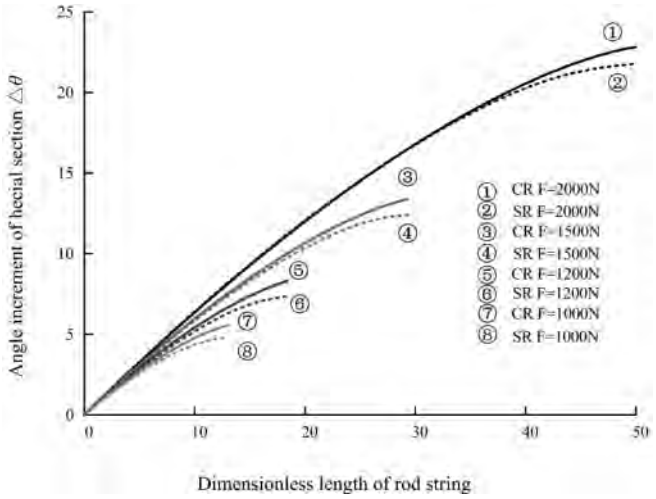

Fig.8 The comparison results of helix angle between simplified and non-simplified equation

5. Conclusions

1. In this paper, a new model based on the entire rod string buckling configuration in vertical well tubing is presented. First, this model is established through a complete, not simplified, buckling equation with weight in four sections. Second, this model is built with a continuity condition at the contact point whose position is variable.
2. The simulation results show that the effect of the boundary condition on the configuration of the helical section and contact force is very little and can be ignored. However, the effects of the boundary conditions, especially at the bottom on the configurations of the suspended sections, are significant.
3. The method for simplifying the equation of the helical section can effect the configuration and contact force of the helical section. Firstly, the contact force located near the beginning of the helical section is different from the complete equation of the helical section; secondly, the angle increment of the helical section is larger than the actual condition.

Acknowledgments

Thanks are due to my tutor Prof. Dong, a respectable, responsible and resourceful scholar, who has provided me with valuable guidance in every stage of the writing of this paper. Thanks are also due for the support of the National Natural Science Foundation of China (Grant No.51174175).

References

1. Lubinski, A. (1950): "A study of the buckling of rotary drilling string," American Petroleum Institute, Jan. 1950.
2. Dong, S.-M. (2003): "Mechanical analysis on causes of worn rod string and tubing of rod pumping wells in the water-flooding oilfield," *Acta Petrolei Sinica*, vol.

24, no. 4, pp. 108–112, July, 2003.

3. Huang, W. J. and Gao, D. L. (2014): "Sinusoidal buckling of a thin rod with connectors constrained in a cylinder," *Journal of Natural Gas Science and Engineering*, vol.18, pp. 237–246, 2014. DOI: 10.1016/j.jngse.2014.03.003.
4. Lubinski, A. (1962): "Althouse W S. Helical buckling of tubing sealed in packers," *Journal of Pertoleum Technology*, vol. 14, no. 6, pp. 655–670, June, 1962. DOI:10.2118/178-PA.
5. Mitchell, R. F. (1982): "Buckling behavior of well tubing: the packer effect," *Society of Petroleum Engineers Journal*, vol. 22, no. 5, pp. 616–624, Oct. 1982. DOI: 10.2118/9264-PA.
6. Jr. Cheatham, B. John (1984): "Helical postbuckling configuration of a weightless column under the action of axial Load," *Society of Petroleum Engineers*, vol. 24, no. 2, pp. 467–472, Aug. 1984. DOI: 10.2118/10854-PA.
7. Sorenson, K.G. and Cheatham Jr, J. B. (1986): "Post-buckling behavior of a circular rod constrained within a circular cylinder," *Journal of Applied Mechanics*, vol. 53, no. 4, pp. 929–934, Dec. 1986.
8. Liu, F. W., Xu, B. Y. and Gao, D. L. (1999): "Packer effect analysis of helical buckling of well tubing," *Journal of Tsinghua University: Science&Technology*, vol. 39, no. 8, pp. 105–108, 1999.
9. Huang, W. J. and Gao, D. L. (2014): "Helical buckling of a thin rod with connectors constrained in a cylinder," *International Journal of Mechanical Sciences*, vol. 84, pp. 189–198, July, 2014. DOI: 10.1016/j.ijmecsci.2014.04.022.
10. Gao, G. H., Li, Q. and Zhang, J. R. (1996): "Buckling analysis of pipe string in a vertical bore hole," *Xi'an Petroleum Institute (Natural Science Edition)*, vol.11, no.1, pp. 33–35, 1996.
11. Hishida, H., Ueno, M., Higuchi, K. and Hatakeyama, T. (1996): "Prediction of helical/sinusoidal buckling," *SPE Petroleum Engineers*, Jan. 1996. DOI: 10.2118/36384-MS.
12. Mitchell, R. F. (1988): "New concepts for helical buckling," *SPE Society of Petroleum Engineers*, vol. 3, no. 3, Sep. 1988. DOI: 10.2118/15470-PA.
13. Mitchell, R. F. (1997): "Effect of well deviation on helical buckling," *SPE Drilling and Completion*, vol. 12, no. 1, pp. 63–69, March, 1997. DOI: 10.2118/29462-PA.
14. Mitchell, R. F. (1999): "Helical buckling of pipe with connectors," SPE Drilling Conference, Amsterdam, Netherlands, March, 1999. DOI: 10.2118/52847-MS.
15. Mitchell, R. F. (2000): "Helical buckling of pipe with connectors in vertical wells," *SPE Drillling and Completion*, vol. 15, no. 3, pp. 162–166, Sep. 2000. DOI: 10.2118/65098-PA.
16. Tan, M. L., Gan, L. F. and Wang, X. W. (2007): "Nonlinear helical buckling of drillstring in inclined wellbore," *Engineering Mechanics*, vol. 24, no. S2, pp. 199–202, 2007.
17. Huang, W. J., Gao, D. L. and Liu, Y. H. (2016): "A study of tubular string buckling in vertical wells," *International Journal of Mechanical Sciences*, vol. 118, pp.231–253, Nov. 2016. DOI: 10.1016/j.ijmecsci.2016.09.035.

LITHOLOGY PREDICTION AND PORE FLUID DETECTION OF TIGHT SANDSTONE RESERVOIR

Continued from page 114

13. Hossain, Z., Mukerji, T., Dvorkin, J. and Fabricius, I. L. (2011): "Rock physics model of glauconitic greensand from the North Sea," *Geophysics*, vol. 76, no. 6, pp. E199–E209, 2011.
14. Jiang, L., Wen, X. T., Zhou, D. H., He, Z. H. and He, X. L. (2012): "The constructing of pore structure factor in carbonate rocks and the inversion of reservoir parameters," *Applied Geophysics*, vol. 9, no. 2, pp. 223–232, 2012.
15. Chen, J., Zheng, Y., Li, Y. and Yan, J. (2015): "Influence on deposition of the three gorges reservoir caused by the reservoirs built upstream," *International Journal of Heat and Technology*, Vol. 33, No. 2, pp. 63-68, 2015.
16. He, F. B., You, J. and Chen, K.Y. (2011): "Gas sand distribution prediction by prestack elastic inversion based on rock physics modeling and analysis," *Applied Geophysics*, vol. 8, no. 3, pp. 197–205, 2011.
17. Dou, Y. T., Shi, S. Q. and Liu, H. Q. (2013): "Prestack inversion method based on FOA," *OGP*, vol. 48, no. 6, pp. 948–953, 2013.